Supplementary Materials for CompuCell3D Model of Cell Migration Reproduces Chemotaxis

Pedro C. Dal-Castel[1], Gilberto L. Thomas[1], Gabriel C. Perrone[1], and Rita M.C. de Almeida[1,2,3*]

[1] *Instituto de Física, Universidade Federal do Rio Grande do Sul, Porto Alegre, RS, Brazil*

[2] *Instituto Nacional de Ciência e Tecnologia: Sistemas Complexos, Universidade Federal do Rio Grande do Sul, Porto Alegre, RS, Brazil and*

[3] *Programa de Pós-Graduação em Bioinformática, Instituto Metrópole Digital, Universidade Federal do Rio Grande do Norte, Natal, RN, Brazil*

(Dated: November 8, 2024)

* pdalcastel@gmail.com; glt@if.ufrgs.br; gabriel.perrone@if.ufrgs.br; rita@if.ufrgs.br

I. MORE DETAILS ABOUT HOW THE MODEL WORKS AND JUSTIFICATIONS

1. *Original Model:*

In the lattice, an object is a set of voxels (3D pixels) with same labels. The model assigns two labels to each lattice site: σ indicates the cell and τ discriminates compartments. This way, different parts of the cell behave differently.

A global energy E is attributed to the lattice configuration. The algorithm randomly chooses a pair of neighboring sites and the labels of the first site of the pair is tentatively copied over the second site. When this change decreases the system energy, the copy is accepted. When this change increases the energy by ΔE, the copy is accepted with probability

$$P_{Boltzmann} = e^{-\frac{\Delta E}{T_B}} \quad , \tag{S1}$$

where T_B is a Boltzmann-like temperature parameter, associated to membrane fluctuations [1]. After this process, a new pair of sites is chosen and the same routine is repeated. A Monte Carlo Step (MCS) is defined as N_{MCS} repetitions of the above process, where N_{MCS} equals the total number of voxels in the lattice.

The model proposed by Fortuna and collaborators [2] considers that the energy of a given configuration is the sum of contact and volume terms, such that

$$E_{total} = E_{contact} + E_{volume} \quad , \tag{S2}$$

where

$$E_{contact} = \sum_{\vec{i}} \sum_{\langle \vec{j} \rangle_{\vec{i}}} J(\tau(\vec{i}), \tau(\vec{j})) \quad , \tag{S3}$$

and

$$E_{volume} = \sum_{\sigma} \lambda_{\sigma} (V^{\sigma}_{current} - V^{\sigma}_{target})^2 \quad . \tag{S4}$$

Here, $J(\tau(\vec{i}), \tau(\vec{j}))$ is the energy per edge between neighboring sites $\vec{i}$ and $\vec{j}$, each with different labels τ. The expression $\langle \vec{j} \rangle_{\vec{i}}$ represents the neighboring sites of $\vec{i}$. For neighboring sites of same type, contact energy is set to zero. λ_{σ} is the inverse of σ^{th} cell's compressibility, $V^{\sigma}_{current}$ and V^{σ}_{target} are, respectively, its current and target volumes. These energy terms

jointly play an important role in cell organization, shape and size.

Lamel protrusions are the motors of cell migration. This action can not be described in CPM by a potential energy. Fortuna and collaborators achieved a protrusion behavior via an energy variation term $\Delta E_{protrusive}$, calculated only for Lamel voxels in contact with the substrate. When a copy of a Lamel site $\vec{j}_{Lamel}$ over a medium site at $\vec{i}_{Medium}$ is attempted, an additional energy term is calculated and added to the energy change, simulating the work done by the cell's non-conservative internal processes. This term is

$$\Delta E_{protrusive} = -\lambda_{F-actin}[F(\vec{i}_{Medium}) - F(\vec{j}_{Lamel})] \quad , \tag{S5}$$

where $F(\vec{i}_{Medium}) - F(\vec{j}_{Lamel})$ represents an actin field gradient between the neighboring voxels of Medium and Lamel at sites $\vec{i}$ and $\vec{j}$, respectively. Here, F is the F-actin field, it is a discrete field set to one in Lamel voxels and to zero otherwise. This dynamics favors Lamel growth over Medium rather than over Cyto. Then, a backpropagation of volume interaction takes place: first, the Lamel volume increases due to protrusions, then Cyto grows towards Lamel in an attempt to balance volume energies, which, in turn, favors Medium growth over Cyto in the rear. Finally, the Nuc lags behind, but its high contact energy with Medium pushes it forward. As a consequence of this process, the entire cell moves. Fortuna and collaborators finely tuned the parameters to prevent separation of Lamel and Cyto and other artifacts. This dynamics makes the cell a self polarizing structure with a preferential migration axis that changes direction over time. Furthermore, it mimics a Local Excitation - Global Inhibition (LEGI) dynamics [3–7]: the more Lamel at one region (the more Lamel/Medium interface), the larger the probability of increasing Lamel at that region. The consequent increase in Lamel, on the other hand, decreases the probability of growing Lamel everywhere else. For more details, see Refs. [2, 8, 9].

Cell kinetics resulting from the model described in Ref. [2] agrees with experiments for cells in the absence of external fields. The model, however, does not have any mechanism to promote cell response to environmental cues. In the next topic, we show an adaptation of this simulation to model chemotactic response.

2. Modified Model: Chemotaxis

Eukaryotic cell migration requires cell cytoskeleton organization. In several eukaryotic cell species, PI_3K, PIP_3, Rac and Rho GTPases implement a Local Excitation Global Inhibition (LEGI) dynamics [3–7] that regulates lamellipodium polimerization and depolimerization. This way, a large and localized lamellipodium promotes its own localized growth, while inhibiting growth in other locations. For more details, see Ref. [10].

In chemotaxis, some chemical concentration around the cell presents a gradient that is spatially sensed by the cell. This signal is biochemically transduced and perturbs cell's internal machinery, favoring a given orientation for lamellipodium growth, directing migration. Here we adapt the model to simulate this three-step dynamics (sensing, reorientation and migration [11, 12]).

We define a linear constant external chemical field $Q(\vec{i})$, whose concentration is sensed in the cell base, i.e., all voxels of the cell (Cyto or Lamel) in the xy plane of $z = 1$. By comparing local concentrations to the average concentration sensed by the cell, the cell creates new Lamel voxels in higher concentration sites. This creation of Lamel increases stability of polarization in the direction of the gradient, which then directs migration. With this dynamics, we aim at a chemotaxis response by reorientation (sometimes referred as compass model [13, 14]) rather than an explicit force acting over the cell. The implementation of the following dynamics in CC3D can be accessed and downloaded from GitHub [15].

To control the production of Lamel voxels in response to chemotaxis, we only allow the creation of new Lamel voxels when Lamel's current volume is below the Lamel average volume taken over the last 100 MCS. This memory mechanism can be expressed by a switch function

$$Switch = \frac{\langle \phi_f \rangle_{n-100}^{n} - \phi_f^n}{|\langle \phi_f \rangle_{n-100}^{n} - \phi_f^n|} \quad , \tag{S6}$$

where ϕ_f^n is Lamel's volume fraction (relative to cell's volume) at time step n, and $\langle \phi_f \rangle_{n-100}^{n}$ is the average of ϕ_f^n over the previous 100 steps. With this memory mechanism active, cell's chemotactic response persists in time. In real cells, actin polymerization is backed by time persistent auxiliary mechanism such as cytoskeleton polarization and non uniform distribution of myosin, integrins and several migration signals within the cell [16]. These intracellular processes allow persistent cell migration. Our choice of 100 MCS is an intermediate value between the regime of pure Potts fluctuations (10 MCS or lower) and the regime

of cell migration persistence (1000 MCS or higher).

Merging the sensing and the memory mechanisms in a single equation, the probability $P_{convert}$ of a Cyto's voxel conversion to Lamel is given by

$$P_{convert}(\vec{i}) = \rho \left[\tanh\left(\mu \frac{Q(\vec{i}) - \langle Q \rangle_{cell}}{\sigma_{Q,cell}} \right) + 1 \right] \times Switch \, . \tag{S7}$$

The first factor on the r.h.s. accounts for the directionality in the Lamel creation at Cyto's base. The external field $Q(\vec{i})$ is evaluated at every voxel $\vec{i}$ at the cell's base and $\langle Q \rangle_{cell}$ is its spatial average. The difference between the value of $Q(\vec{i})$ and the field's average determines the likelihood that a Cyto's voxel will switch to Lamel at position $\vec{i}$. The μ parameter is the hyperbolic tangent steepness at $Q(\vec{i}) - \langle Q \rangle_{cell} = 0$, it regulates the asymmetry in Lamel voxel creation. The argument is normalized by the standard deviation of the field $\sigma_{Q,cell} = \sqrt{\langle Q^2 \rangle_{cell} - \langle Q \rangle_{cell}^2}$ so that μ stands for both field gradient intensity and cell's susceptibility. At last, ρ normalizes the probability, so it assumes value $\rho = 1/2$. This equation does not participate in the calculation of the voxel copy probabilities, it controls the creation of new Lamel pixels and works independently of Eq. S1. The second factor is the switch we defined in Eq. S6. Both factors together regulate directionality of Lamel creation and persistent response through time. After sensing and reorienting, the F-actin promoted protrusions in Lamel accomplishes the third step of the chemotactic response, i.e., migration. This model achieves chemotactic response as show the cell trajectories.

II. MEAN VELOCITY ANALYSIS USING LOG SCALE IN BOTH AXES

The divergence of $\langle |V_\perp| \rangle$ and $\langle |V_\parallel| \rangle$ for $\delta \to 0$ might not be clear in the figure we chose for the main manuscript. By using logarithmic scales in both axes, this behavior is more clear. We chose to use linear scale in the original figure so that the $\langle V_\perp \rangle$ curve could also be shown. In this version, we deleted the $\langle V_\perp \rangle$ curves to allow logarithmic scale in both axes.

In double log scale, the $\langle |V_\perp| \rangle$ and $\langle |V_\parallel| \rangle$ curves are lines with negative angular coefficient for small δ. This is characteristic of power laws with negative exponent. Therefore, these curves diverge in the linear scale when $\delta \to 0$. We can only guarantee this behavior for time intervals above 1 MCS, because this is our lower time step limit.

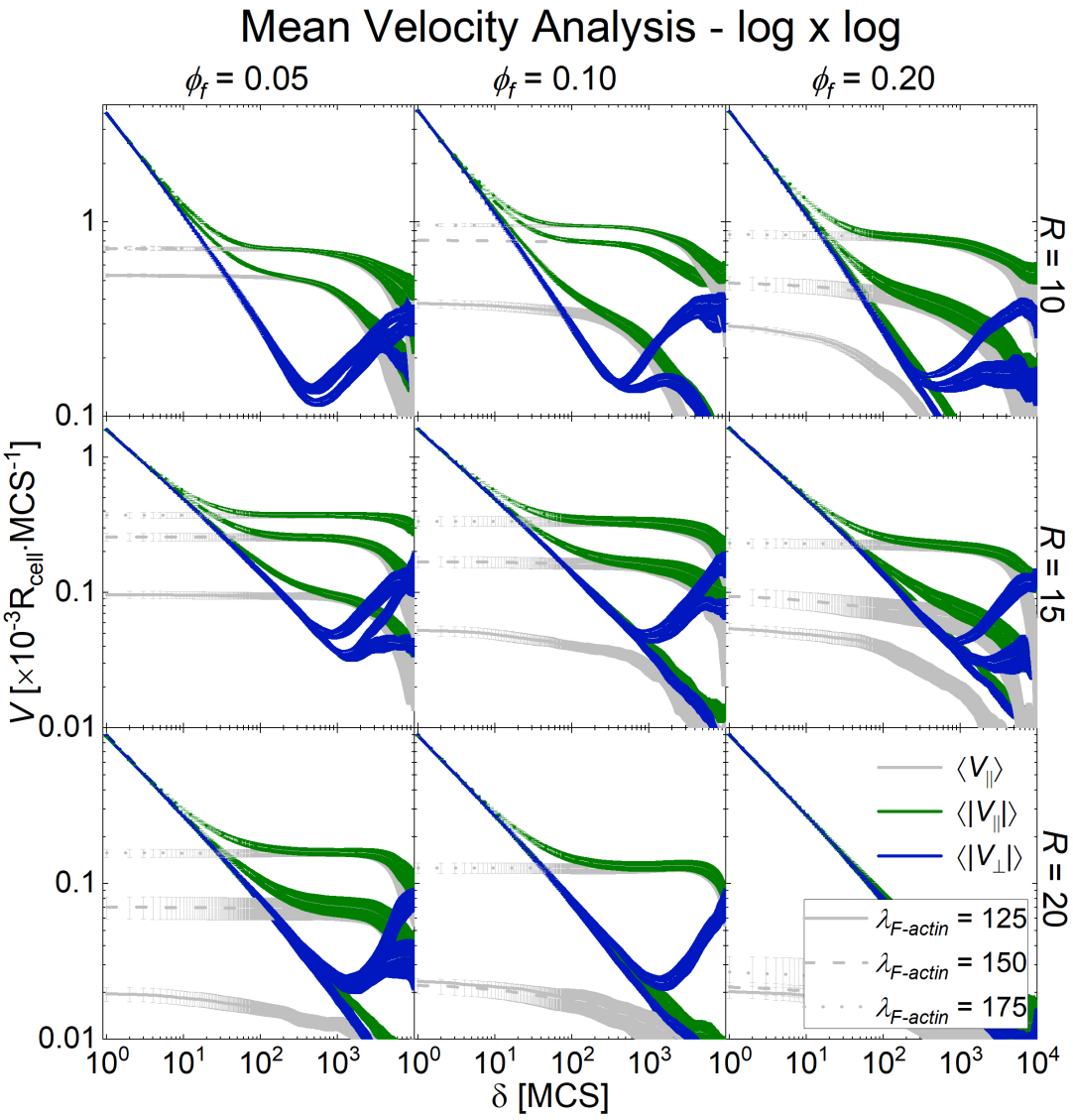

Figure S7. Mean Velocity Analysis using Log scale in both axes. Plots show divergence of $\langle|V_\perp|\rangle$ and $\langle|V_\parallel|\rangle$.

III. INPUT PARAMETERS AND RESULTS TABLES

Table S1 presents the results of MSD fits and drift speed for cell radius $R = 10$, zero chemotactic response $\mu = 0$, protrusion strength $\lambda_{F-actin} = \{125, 150, 175\}$ and Lamel volume fraction $\phi_F = \{0.05, 0.10, 0.20\}$. The MSD fit yields slow diffusion coefficient $D[R^2/\text{MCS}]$, the S parameter and the persistence time $P[\text{MCS}]$. S parameter is the time interval that separates the first diffusive regime and the ballistic-like regime in natural units. It also relates to the fast diffusion coefficient $A = \frac{2DS}{1-S}$. The drift speed V_d is obtained from the average of velocity component parallel to polarization for smallest time interval, as we defined in Eq.

(11).

Table S2 presents the results of MSD fits, drift speed, terminal speed and chemotactic efficiency for cell radius $R = 10$, saturated chemotactic response $\mu = 10^6$, protrusion strength $\lambda_{F-actin} = \{125, 150, 175\}$ and Lamel volume fraction $\phi_F = \{0.05, 0.10, 0.20\}$. We find $B[R^2/\mathrm{MCS}^2]$, the parameter of the last ballistic regime associated to chemotactic response. The terminal speed $V_T[R/\mathrm{MCS}] = \sqrt{B}$ is the cell speed for large time intervals during chemotactic response, and chemotactic efficiency $\varepsilon = \frac{V_T}{V_d}$ is the ratio between terminal speed and drift speed.

Table S1. Results for simulations with parameter inputs: $R = 10$, $\mu = 0$, $\lambda_{F-actin} = \{125, 150, 175\}$, and $\phi_F = \{0.05, 0.10, 0.20\}$.

$R = 10 \quad \mu = 0$					
ϕ_f	$\lambda_{F-actin}$	$D[R^2/\mathrm{MCS}]$	$P[\mathrm{MCS}]$	S	$V_d[R/\mathrm{MCS}]$
0.05	125	4.18E-04	1.30E+03	8.39E-01	5.32E-04
0.05	150	1.88E-03	3.52E+03	9.21E-01	7.31E-04
0.05	175	3.16E-03	7.20E+03	9.54E-01	7.37E-04
0.1	125	1.84E-04	1.05E+03	8.08E-01	3.81E-04
0.1	150	1.86E-03	2.90E+03	9.06E-01	8.06E-04
0.1	175	5.40E-03	7.18E+03	9.54E-01	9.65E-04
0.2	125	–	–	–	–
0.2	150	7.18E-04	2.49E+03	8.92E-01	4.86E-04
0.2	175	3.17E-03	4.60E+03	9.29E-01	8.64E-04

Table S2. Results for simulations with parameter inputs: $R = 10$, $\mu = 10^6$, $\lambda_{F-actin} = \{125, 150, 175\}$, and $\phi_F = \{0.05, 0.10, 0.20\}$.

$R = 10 \quad \mu = 10^6$								
ϕ_f	$\lambda_{F-actin}$	$D[R^2/\mathrm{MCS}]$	$P[\mathrm{MCS}]$	S	$B[R^2/\mathrm{MCS}^2]$	$V_d[R/\mathrm{MCS}]$	$V_T[R/\mathrm{MCS}]$	ε
0.05	125	3.20E-04	1.20E+03	5.90E-02	1.07E-07	5.75E-04	3.28E-04	5.70E-01
0.05	150	1.45E-03	3.15E+03	1.33E-02	1.00E-07	7.61E-04	3.17E-04	4.16E-01
0.05	175	4.79E-03	9.27E+03	3.97E-03	3.97E-08	7.47E-04	1.99E-04	2.67E-01
0.1	125	1.85E-04	9.95E+02	9.78E-02	2.32E-08	4.49E-04	1.52E-04	3.39E-01
0.1	150	1.73E-03	2.76E+03	1.11E-02	4.61E-08	7.83E-04	2.15E-04	2.74E-01
0.1	175	6.80E-03	7.15E+03	2.80E-03	2.88E-08	9.72E-04	1.70E-04	1.74E-01
0.2	125	–	–	–	–	–	–	–
0.2	150	7.54E-04	2.58E+03	2.51E-02	9.69E-09	5.14E-04	9.84E-05	1.91E-01
0.2	175	3.19E-03	3.69E+03	5.87E-03	1.49E-08	9.13E-04	1.22E-04	1.34E-01

IV. 4-REGIMES MSD FIT STEP-BY-STEP WITH EXAMPLE

Fitting an MSD curve can be difficult due to the multiple regimes for very different time scales. Some parameters depend on each other and it can be hard to separate them. A direct implementation of a gradient descent algorithm may not give the best result, even if you weight the data appropriately.

Here we present a step-by-step fitting procedure of Eq. S8

$$\langle|\Delta\vec{r}|^2\rangle = 2D(\Delta t - P(1 - e^{-\Delta t/P})) + A\Delta t + B\Delta t^2 \quad . \tag{S8}$$

over a simulated MSD data that presents all four regimes of movement (short time diffusive, intermediate ballistic, long term diffusive and long term ballistic), as shown in Fig. S8.

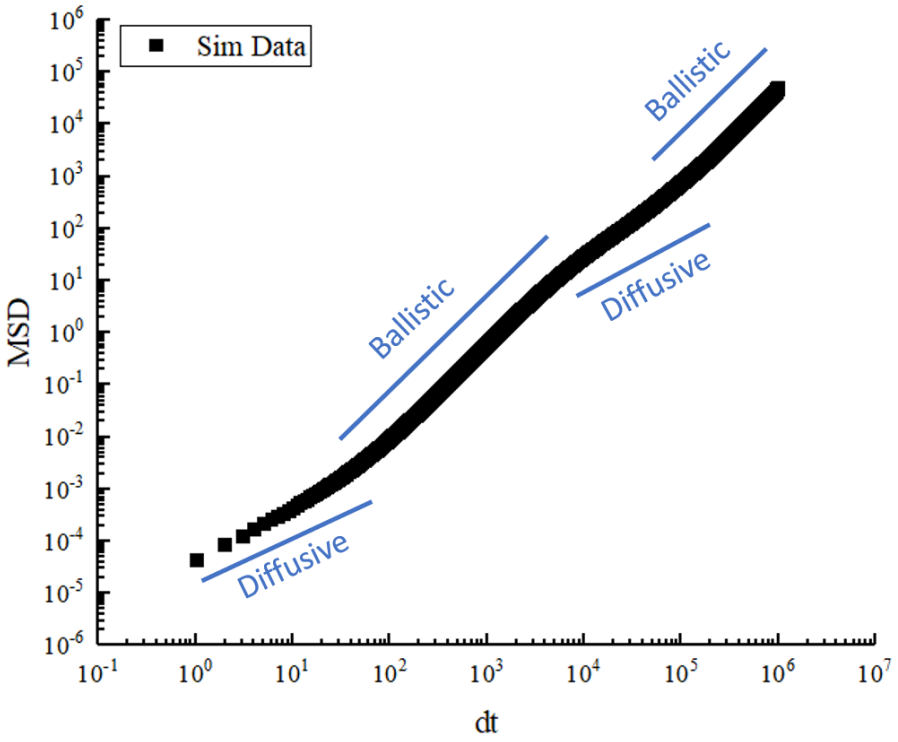

Figure S8. Plot of MSD vs Δt in log-log scale.

This method yields good fits, although it is more complicated than simply hitting "the fit button" on a data analysis software, but it is faster and less arbitrary than the brute force iterative fitting in each curve region. You only need access to basic data manipulation and basic gradient descent fitting routine.

We start with a MSD vs Δt in log-log scale, as shown in Fig. S8. This curve is the

particular case $R = 10$, $\phi_F = 0.10$, $\lambda_{F-actin} = 150$. We obtained the given curve by averaging the MSDs of 10 different cell trajectories.

The first parameter to extract is B. It is the easiest since the squared term is dominant for large Δt. We take advantage of this fact: by differentiating our MSD function given in Eq. S8 and taking the limit for large Δt:

$$\begin{aligned} MSD_t &= \frac{d}{d(\Delta t)}\langle|\Delta\vec{r}|^2\rangle = 2D(1 - e^{-\Delta t/P}) + A + 2B\Delta t \quad , \\ \lim_{\Delta t\to\infty} MSD_t &= 2B\Delta t \quad , \end{aligned} \tag{S9}$$

Only parameter B remains. Then, we take the numerical derivative of our MSD simulated data and plot it linearly, as we show in Fig. S9. From the graph, we identify the straight-line region, whose slope must be equal to $2B$. A linear fit of this region, shown by a red line, determines B.

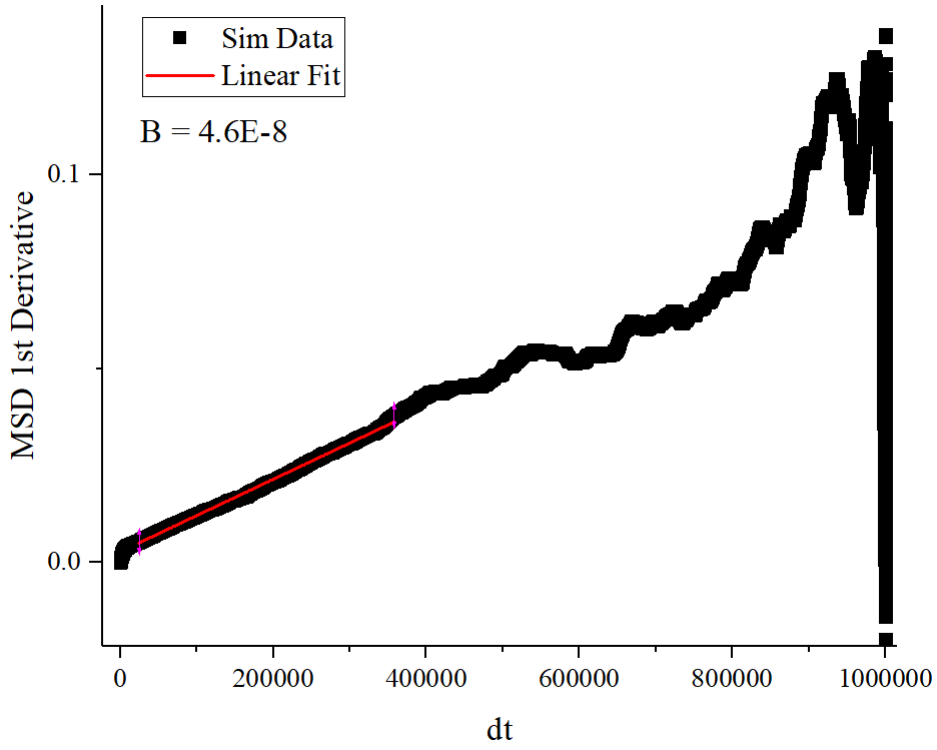

Figure S9. Plot and linear fit of the linear region in the 1st differentiated MSD curve (linear scale).

After we found the parameter B, we replot MSD $- B\Delta t^2$ in Fig. S3. We can see that this subtraction eliminates the long-term ballistic regime, and the plotted curve resembles the MSD in the absence of the chemotactic field.

The procedure for fitting the remaining parameters have already been published by Fortuna and collaborators in 2020 [2]. For the sake of completeness, we will reproduce it here.

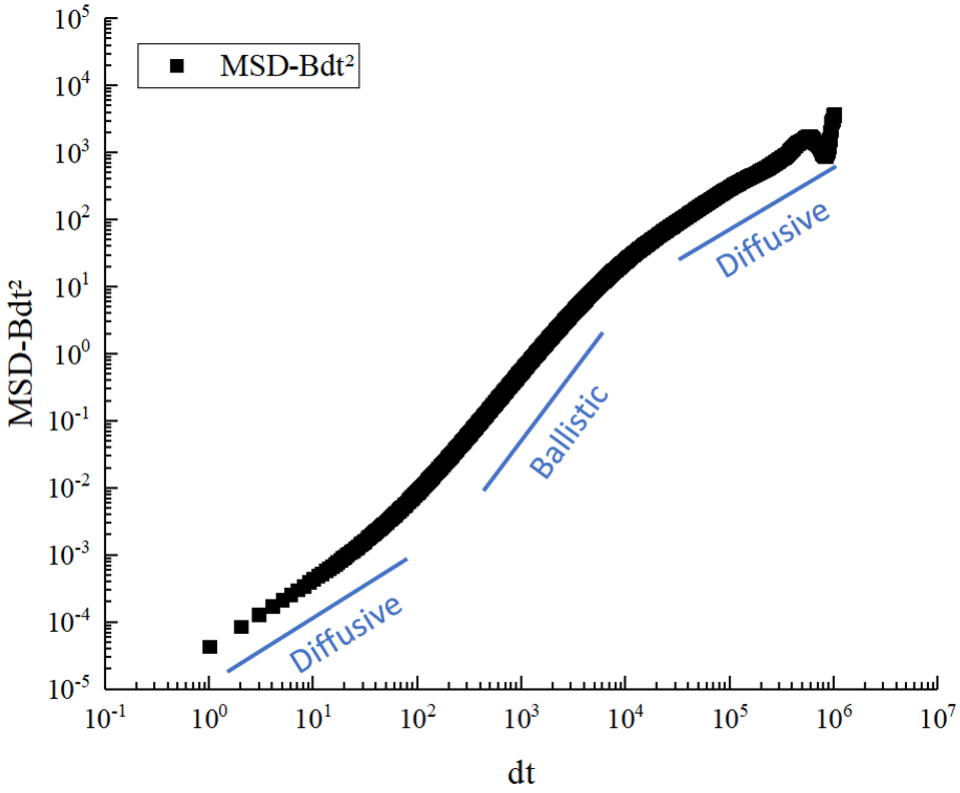

Figure S9. MSD without the ballistic term $B\Delta t^2$.

The reduced MSD equation now is

$$\langle|\Delta\vec{r}|^2\rangle = 2D(\Delta t - P(1 - e^{-\Delta t/P})) + A\Delta t \quad , \tag{S10}$$

and we have to find the parameters A, D, and P.

We differentiate Eq. S10 twice in respect to Δt to get rid of the linear term $A\Delta t$, resulting

$$\mathrm{MSD}_{tt} = \frac{d^2}{d(\Delta t)^2}\langle|\Delta\vec{r}|^2\rangle = \frac{2D}{P}e^{-\Delta t/P} \, . \tag{S11}$$

So, the $\log(\mathrm{MSD}_{tt}) \times \Delta t$ plot should show a curve region with linear behavior. The linear fitting of this region will determine parameters D and P.

Fig S4 presents the time-differentiated simulated data with black squares. The blue line is the smoothed curve for the data. It helps us to identify the linear region. In this region, we perform a nonlinear curve fit using Eq. S11 to find parameters D and P.

Subtracting from original MSD both Fürth and chemotactic terms, we are left with the

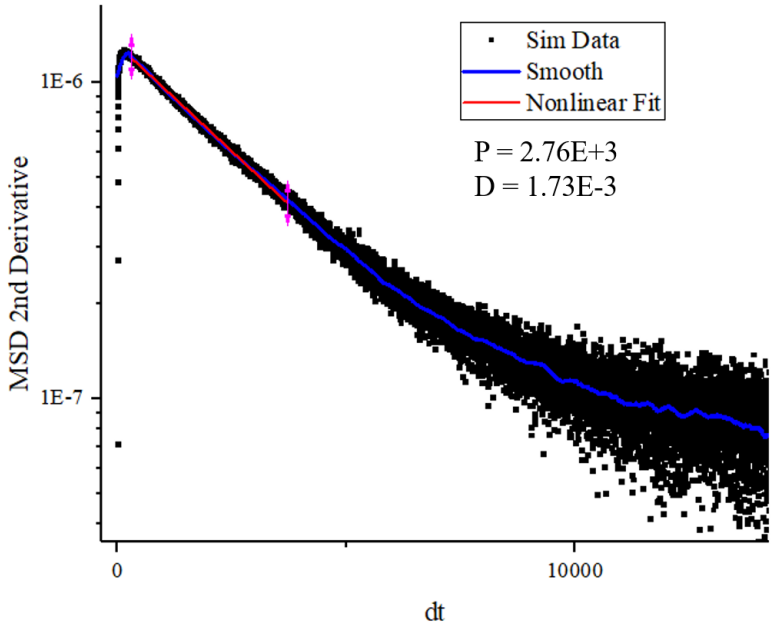

Figure S11. Plot and nonlinear fit (using Eq. S11) of MSD 2nd derivative to find parameters D and P. Graph scales are log-linear.

linear term $A\Delta t$, *i.e.*,

$$A\Delta t = \text{MSD} - 2D(\Delta t - P(1 - e^{-\Delta t/P})) - 2B\Delta t^2 \quad . \tag{S12}$$

This subtraction in the simulated MSD data gives us the curve presented with black squares in Fig. S12.

Fixing the intercept coefficient at zero, we perform a linear fit for the small Δt region. The resulting fitting is presented by the red line in Fig. S12. Note that for this fitting, it does not matter if the graph is put in log-log or linear-linear scales (it looks like a straight line in both choices), provided that you perform a linear fit in the original coordinate system.

With all 4 parameters, we can plot both MSD simulated data points and the final fit curve. This is showed in Fig. S12. As you may have noticed, not all steps are user independent, different decisions will impact the final result, for example: 1) what exactly is the range of data points I have to set in each fit step? 2) do I ignore this noisy part? 3) do I ignore this curvy part in my supposedly linear region? 4) in which order do I fit the parameters? 5) do I repeat the process for some of the parameters? The first consideration is that no model will perfectly fit the data. To be practical, we don't care about obtaining precise parameter values as much as we care about the relationship between the fitting parameters and cell

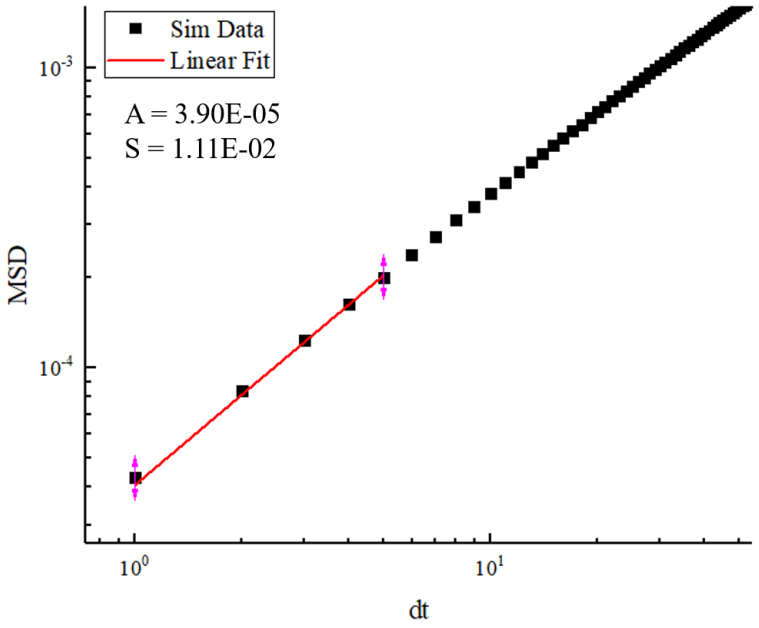

Figure S12. MSD curve only with the remaining $A\Delta t$ term. The relation between S and A is $A = \frac{2DS}{1-S}$.

behavior. For example: cells with clear and stable polarization should present higher P relative to those with less stable polarization; cells that walk longer distances over same periods of time should present a higher D relative to those that do not move as much; cells that present higher fluctuations in its structure should present a higher A; and cells that walk faster towards a chemical field source should present a higher B. Precise estimates are not the goal and may even not be possible to achieve in any way. The real requirements are: the procedure is 1) standardized, 2) reproducible, and 3) the results must correlate with observed cell behavior.

BIBLIOGRAPHY

[1] Maciej Swat, Gilberto L. Thomas, Julio Monti Belmonte, Abbas Shirinifard, Dimitrij Hmeljak, and James A. Glazier. Multi-scale modeling of tissues using compucell3d. *Methods in Cell Biology*, 110:325–366, 2012.

[2] Ismael Fortuna, Gabriel C Perrone, S Krug, Monique, Eduarda Susin, Julio M Belmonte, Gilberto L Thomas, Glazier James A, and Rita M C de Almeida. Compucell3d simulations reproduce mesenchymal cell migration on flat substrates. *Biophysical J.*, 118(11):2801–2815, 2020.

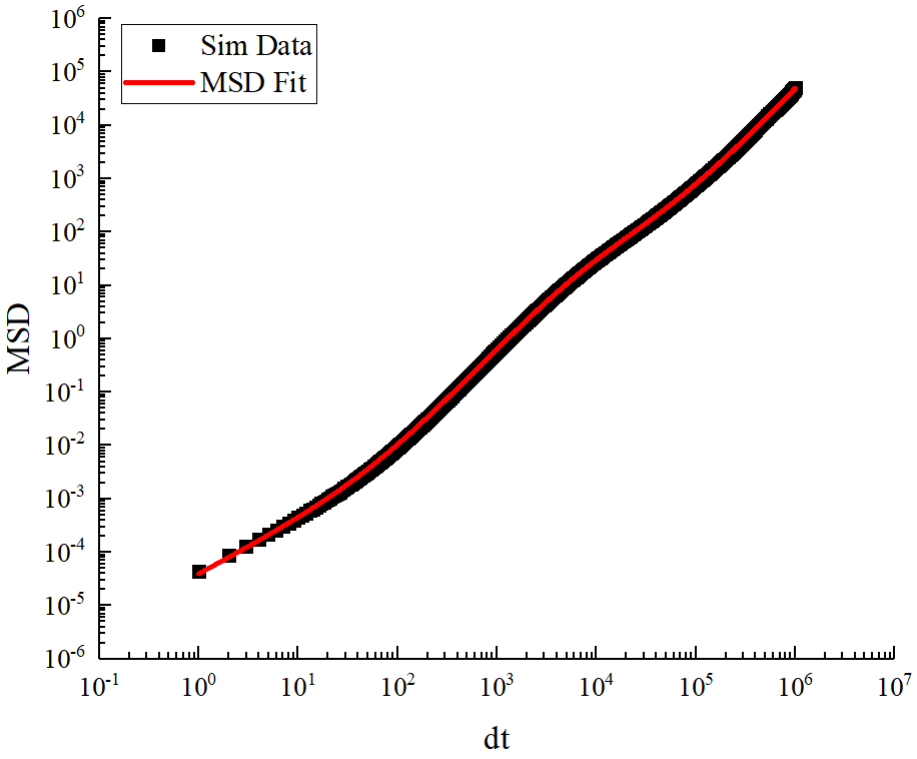

Figure S12. Final MSD fit in log-log scale.

[3] A. M. Turing. The chemical basis of morphogenesis. *Phil. Trans. R. Soc. Lond. B*, 237:37–72, 1952.

[4] Kristen F. Swaney, Chuan-Hsiang Huang, and Peter N. Devreotes. Eukaryotic chemotaxis: A network of signaling pathways controls motility, directional sensing, and polarity. *Annual Review of Biophysics*, 39(1):265–289, apr 2010.

[5] Orion D. Weiner, Paul O. Neilsen, Glenn D. Prestwich, Marc W. Kirschner, Lewis C. Cantley, and Henry R. Bourne. A PtdInsP3- and rho GTPase-mediated positive feedback loop regulates neutrophil polarity. *Nature Cell Biology*, 4(7):509–513, jun 2002.

[6] Chang Y. Chung and Richard A. Firtel. Signaling pathways at the leading edge of chemotaxing cells. *Journal of Muscle Research and Cell Motility*, 23(7/8):773–779, 2002.

[7] Carol L. Manahan, Pablo A. Iglesias, Yu Long, and Peter N. Devreotes. Chemoattractant signaling in dictyostelium discoideum. *Annual Review of Cell and Developmental Biology*, 20(1):223–253, nov 2004.

[8] Gilberto L Thomas, Ismael Fortuna, Gabriel C Perrone, Glazier James A, Julio M Belmonte, and Rita M C de Almeida. Parameterizing cell movement when the instantaneous cell migration velocity is ill-defined. *Physica A*, 550:124493, 2020.

[9] Gilberto L. Thomas, Ismael Fortuna, Gabriel C. Perrone, François Graner, and Rita M.C. de Almeida. Shape–velocity correlation defines polarization in migrating cell simulations. *Physica A: Statistical Mechanics and its Applications*, 587:126511, feb 2022.

[10] Miguel Vicente-Manzanares and Alan Rick Horwitz. Cell migration: An overview. In *Methods in Molecular Biology*, pages 1–24. Humana Press, 2011.

[11] Evanthia T. Roussos, John S. Condeelis, and Antonia Patsialou. Chemotaxis in cancer. *Nature Reviews Cancer*, 11(8):573–587, jul 2011.

[12] Tian Jin, Xuehua Xu, and Dale Hereld. Chemotaxis, chemokine receptors and human disease. *Cytokine*, 44(1):1–8, oct 2008.

[13] Henry R. Bourne and Orion Weiner. Cell polarity: A chemical compass. *Nature*, 419(6902):21–21, sep 2002.

[14] Matthew P. Neilson, Douwe M. Veltman, Peter J. M. van Haastert, Steven D. Webb, John A. Mackenzie, and Robert H. Insall. Chemotaxis: A Feedback-Based Computational Model Robustly Predicts Multiple Aspects of Real Cell Behaviour. *PLoS Biol.*, 9(5):e1000618, May 2011.

[15] P. C. Dal-Castel. Single cell chemotaxis simulation cc3d. `https://github.com/pdalcastel/Single_Cell_Chemotaxis_2.3`, 2023.

[16] Andrew C Callan-Jones and Raphaël Voituriez. Actin flows in cell migration: from locomotion and polarity to trajectories. *Current Opinion in Cell Biology*, 39:12–17, 2016.